Eur. Phys. J. B **46**, 463–469 (2005)
DOI: 10.1140/epjb/e2005-00275-3

THE EUROPEAN PHYSICAL JOURNAL B

First-principles study of the optical properties of $PbTiO_3$

S.M. Hosseini[a], T. Movlarooy, and A. Kompany

Department of Physics, (Electroceramic and Material Laboratory), Ferdowsi University of Mashhad, Iran

Received 6 April 2005
Published online 7 September 2005 – © EDP Sciences, Società Italiana di Fisica, Springer-Verlag 2005

Abstract. The optical properties of $PbTiO_3$ were studied from first principles using the density functional theory. The dielectric functions and optical constants are calculated using the full potential–linearized augmented plane wave (FP-LAPW) method with the generalized gradient approximation (GGA). The theoretical calculated optical properties and energy loss (EEL) spectrum yield a static refractive index of 2.83 and a plasmon energy of 23.1 eV for cubic phase. The effective electron number at low energy saturates near 20 eV with the value of 18.1 for the effective electron number. In the tetragonal phase the static refractive index decreases to 2.59 and yields a plasmon energy of 22.7 eV.

PACS. 31.15.Ar Ab initio calculations – 78.20.-e Optical properties of bulk materials and thin films – 78.20.Ci Optical constants (including refractive index, complex dielectric constant, absorption, reflection and transmission coefficients, emissivity)

1 Introduction

The development of computational methods in the electronic structure community has led to a new class of first principles approaches, based upon a full solution of the quantum mechanical ground state of the electron system within the local-density approximation (LDA) to KohnSham density functional theory (DFT) [1]. In principle, these methods take as their only inputs the atomic numbers of the constituent atoms. The modeling of electronic and optical properties, by means of first-principles calculations, has become a very useful tool for understanding about the structural, electronic and optical properties of the various materials.

Ferroelectric perovskite-type titanates such as $PbTiO_3$ (PT) have various attractive properties from the electrical and optical viewpoint. These include piezoelectric transducers and actuators, nonvolatile ferroelectric memories, dielectrics for microelectronics and wireless communication, pyroelectric arrays, and nonlinear optical applications. In addition, (PT) has a large electro-optic coefficient and high photorefractive sensitivity, therefore can be used as an optical sensor [2]. It is also being seriously considered for many other optical devices. In its low temperature phase, (PT) has tetragonal symmetry and is ferroelectric, which belongs to the *P4mm* symmetry group. At 763 K it undergoes a transition to a cubic and paraelectric state having space group *Pm3m* [3]. However, an understanding of optical properties, from the viewpoint of material science, for this structure is also significant.

In the present work the optical properties of (PT) in both the cubic and tetragonal phases have been studied using the full potential linearized augmented plane wave method (FP-LAPW). The results, in comparison with the published data, are in good agreement with the experimental and previous theoretical results.

2 Method of calculation

Calculation of the optical properties, of (PT) were carried out with a self-consistent scheme by solving the Kohn-Sham equation using a FP-LAPW method in the framework of the DFT along with the generalized gradient approximation (GGA) method [4,5] by WIEN2k codes [6].

In the FP-LAPW method, space is divided into two regions, a spherical "muffin-tin" around the nuclei in which radial solutions of Schrödinger equation and their energy derivatives are used as basis functions, and an "interstitial" region between the muffin tins (MT) in which the basis set consists of plane waves. There is no pseudopotential approximation and core states are calculated self-consistently in the crystal potential. Also, core states are treated fully relativistically while valence and semi-core states are treated semi-relativistically (i.e. ignoring the spin-orbit coupling). The cut-off energy, which defines the separation of the core and valance states, was chosen as –6 Ryd.

The complex dielectric tensor was calculated, in this program, according to the well-known relations [7]:

$$\operatorname{Im}\varepsilon_{\alpha\beta}(\omega) = \frac{4\pi e^2}{m^2\omega^2}\sum_{c,v}\int \mathrm{d}k\langle c_{\mathbf{k}}|p^{\alpha}|v_{\mathbf{k}}\rangle\langle v_{\mathbf{k}}|p^{\beta}|c_{\mathbf{k}}\rangle\delta(\varepsilon_{c_{\mathbf{k}}}-\varepsilon_{v_{\mathbf{k}}}-\omega) \quad (1)$$

[a] e-mail: sma_hosseini@yahoo.com

$$\mathrm{Re}\,\varepsilon_{\alpha\beta}(\omega) = \delta_{\alpha\beta} + \frac{2}{\pi} P \int_0^\infty \frac{\omega' \mathrm{Im}\varepsilon_{\alpha\beta}(\omega')}{\omega'^2 - \omega^2} d\omega' \qquad (2)$$

and the optical conductivity is given by:

$$\mathrm{Re}\,\sigma_{\alpha\beta}(\omega) = \frac{\omega}{4\pi} \mathrm{Im}\varepsilon_{\alpha\beta}(\omega). \qquad (3)$$

In equation (1), c_k and v_k are the crystal wavefunctions corresponding to the conduction and the valance bands with crystal wave vector $\mathbf{k}$ (Fig. 4). In equation (3) the conductivity tensor relating the interband current density j_α in the direction α which flows upon application of an electric field E_β in direction β in which the sum in equation (1) is over all valence and conduction band states labeled by v and c.

Moreover, the complex dielectric constant of a solid is given as:

$$\varepsilon(\omega) = \varepsilon_1(\omega) + i\varepsilon_2(\omega) \qquad (4)$$

Here, real and imaginary parts are related to optical constants $n(\omega)$ and $k(\omega)$ as:

$$\begin{aligned} \varepsilon_1(\omega) &= n^2(\omega) - k^2(\omega) \\ \varepsilon_2(\omega) &= 2n(\omega)k(\omega). \end{aligned} \qquad (5)$$

The other optical parameters, such as energy-loss spectrum and oscillator strength sum rule are immediately calculated in terms of the components of the complex dielectric function [7].

3 Results and discussion

The calculations first were carried out using the experimental data for lattice constants ($a = b = c = 3.95$ Å) in the cubic phase. Then by minimizing the ratio of the total energy of the crystal to its volume (volume optimizing) the theoretical lattice constants were obtained ($a = b = c = 3.98$ Å).

For the tetragonal structure, we used the crystallographic data with lattice constant of $a = b = 3.902$ and $c = 4.156$ Å [3]. The calculated lattice constant after volume optimization is $a = b = 3.944$ and $c = 4.2$ [$c/a = 1.065$, $V_0 = 441.36$ (au)^3].

In order to reduce the time of the calculations we used the symmetries of the crystal structure and some other approximations for simplicity. The calculation was performed with 1000 k-points in the cubic and 300 k-points for the tetragonal phase.

The self-consistent process, for both phases, after 11 cycles had convergence of about 0.0001 in the eigenvalues in which for the cubic phase 559 plane waves and for the tetragonal phase 2971 plane waves were produced. Under these conditions the values of the other parameters were $G_{\max} = 14$, $R_{\mathrm{MT}}(\mathrm{Pb}) = 2.4$ au, $R_{\mathrm{MT}}(\mathrm{Ti}) = 1.7$ au, $R_{\mathrm{MT}}(\mathrm{O}) = 1.6$ au. The iteration halted when the total charge adjustment was less than 0.0001 between steps. The broadening parameters 0.1 eV were chosen for gamma for Lorentz broadening.

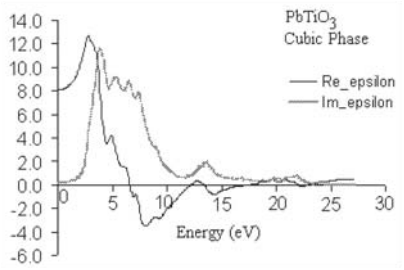

Fig. 1. Real and imaginary part of the dielectric function for (PT) in cubic phase.

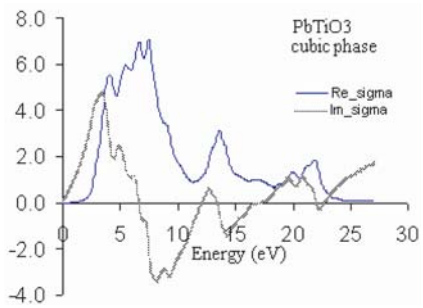

Fig. 2. Real and imaginary part of the of the optical conductivity for (PT) in cubic phase.

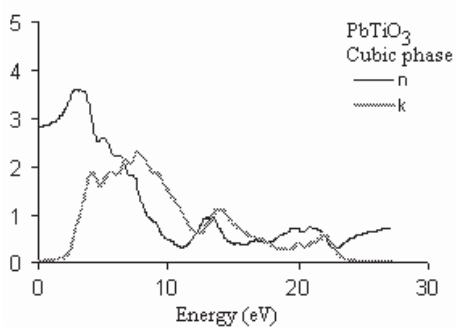

Fig. 3. The optical constants $n(\omega)$ and $k(\omega)$ for (PT) in the cubic phase.

3.1 Paraelectric phase

3.1.1 Dielectric function

We calculated both the electronic and optical properties of (PT) in the cubic phase, but here we only present the optical properties. The detailed description for the electronic properties is given elsewhere [8].

The real and the imaginary parts of the dielectric functions are shown in Figure 1 for (PT) in the cubic phase. The value of the main peak of $\varepsilon_1(\omega)$ curve is 12.68 at energy of 2.74 eV and for $\varepsilon_2(\omega)$ is 11.51 at the energy equal 3.89 eV.

The real and the imaginary parts of optical conductivity are shown in Figure 2 for (PT) in cubic phase.

In Figure 3 the optical constant $n(\omega)$ and $k(\omega)$ is shown for (PT) in cubic phase.

Table 1. Refractive index in cubic phase calculated by various methods.

Methods	Refractive index (n)
Experimental [10] at 589 nm	$\sim$2.94 ($\varepsilon = 8.64$)
Theory	
FP-LDA [9] (static)	$\sim$2.87(ε_0=8.24)
FP-LAPW (GGA96) (static) (this work)	$\sim$2.83($\varepsilon_0 = 8.1$)
FP-LAPW (GGA96) at 588 nm (this work)	$\sim$2.87 ($\varepsilon = 8.25$)

The static refractive index value for (PT) in the cubic phase calculated in this work, and the values obtained by other methods are summarized in Table 1.

Referring to Table 1, it can be seen that the calculated refractive index in this work is smaller than the values measured experimentally. This difference may be mainly due to the calculated band gap value 1.7 eV (without empirical correction factor) in which is smaller than the reported experimental band gap value, 3.0–4.5 eV [11].

3.1.2 Electron energy loss spectroscopy

EELS is a valuable tool for investigating various aspects of materials [12]. It has the advantage of covering the complete energy range including non-scattered and elastically scattered electrons (Zero Loss). At intermediate energies (typically 1 to 50 eV) the energy losses are due primarily to a complicated mixture of single electron excitations and collective excitations (plasmons). The positions of the single electron excitation peaks are related to the joint density of states between the conduction and valence bands, whereas the energy required for the excitation of bulk plasmons depends mainly on the electron density in the solid. Here electrons, which excite the atoms electrons of the outer shell is called Valence Loss or valence interaband transitions (Fig. 4). At higher energies, typically a few hundred eV, edges can be seen in the spectrum, indicating the onset of excitations from the various inner atomic shells to the conduction band. In this case the fast electrons excite the inner shell electrons (Core Loss) or induce core level excitation of Near Edge Structure (ELNES) and XANES. The edges are characteristic of particular elements and their energy and height can be used for elemental analysis.

In the case of interband transitions, which consist mostly of plasmon excitations, the scattering probability for volume losses is directly connected to the energy loss function. One can then calculate the EEL spectrum from the following relations [7]:

$$\varepsilon_{\alpha\beta}(\omega) = \varepsilon_1 + i\varepsilon_2 \text{ and } EELSpectrum = \mathrm{Im}[-1/\varepsilon_{\alpha\beta}(\omega)] = \frac{\varepsilon_2}{\varepsilon_1^2 + \varepsilon_2^2}. \quad (6)$$

In Figure 5 the energy loss function is plotted for (PT) in cubic phase. These peaks can, however, have different origins such as charge carrier plasmons and interband or intraband excitations. The energy of the maximum peak of $\mathrm{Im}[-\varepsilon^{-1}(\mathrm{E})]$ at 22.9 eV is assigned to the energy of the volume plasmon $\hbar\omega_p$. The first peak at 11.7 eV and

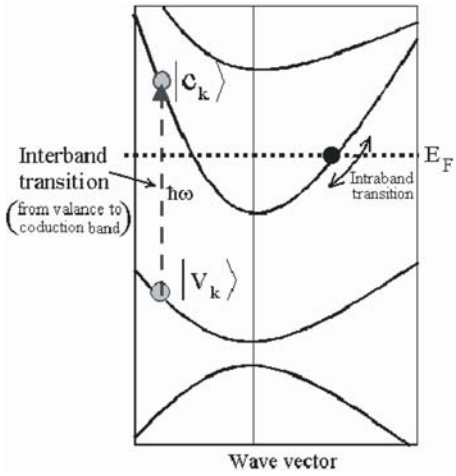

Fig. 4. Valence interbands transitions.

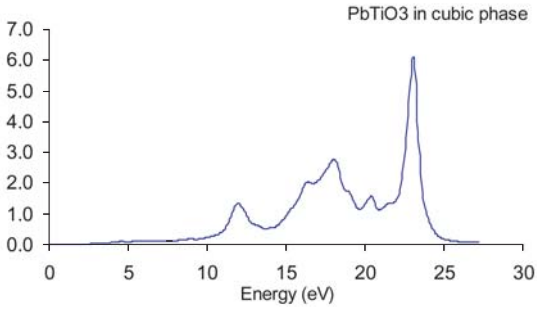

Fig. 5. Electron energy loss spectrum $\mathrm{Im}[-\varepsilon^{-1}(\mathrm{E})]$ for PT in cubic phase.

second peak at 18 eV originates from O-2p to Ti-3d and Pb-6p orbitals, respectively. The value of $\hbar\omega_p$ obtained in this work and for free electron is given in Table 2.

For free electrons the plasmon energy is calculated according to the following model:

$$\hbar\omega_p^e = \hbar\sqrt{\frac{ne^2}{\varepsilon_0 m}}. \quad (7)$$

If we use this model, then what should be the number of valance electrons per (PT) molecule, N, used to calculate the density of valance electrons, n, and thus the plasmon energy in equation (7)? The partial DOS from the Pb, Ti and O atoms are shown in Figure 6. From the PDOS of the Pb and O-atoms it can be seen that the Pb-5d and O-2s state has a narrow band separated from the upper valance band by nearly–11 eV, therefore the participation of the Pb-5d and O-2s states in the volume plasmon excitation

Table 2. (PT) plasmon energy $\hbar\omega_p$ of the energy loss function in cubic phase calculated by this method and free electron.

Methods	Plasmon energy $\hbar\omega_p$(eV)
FP-LAPW (GGA96) (this work)	∼23.1
Free electron (ignoring Pb-5d and O-2s states)	∼26.5
Free electron	∼33.0

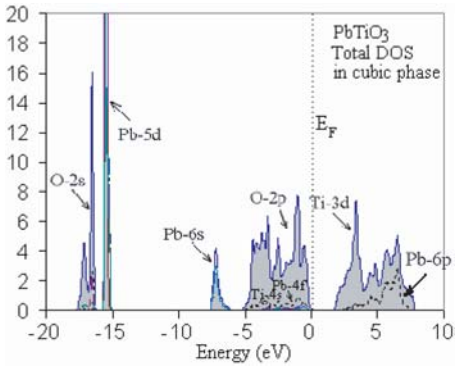

Fig. 6. The total DOS of (PT) in cubic phase. The zero of the energy was set at the top of valance band.

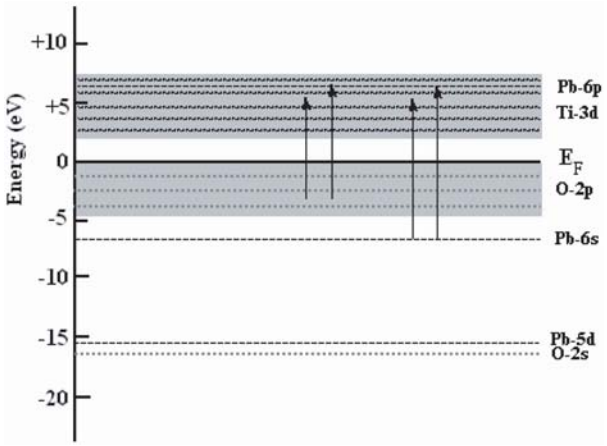

Fig. 7. Simplified energy level diagram for transitions from valance to conduction band at low energy for $PbTiO_3$.

at low energies are rather weak. If we take only the contribution of $4f^{14}$, $6s^2$ and $6p^2$ electrons of Pb, $3d^2$ and $4s^2$ of Ti and $2p^4$ of O (ignoring the contribution of $5d^{10}$ and $2s^2$ electron of Pb and O atom respectively) then we have $N = 34$ and the free electron plasmon energy will be 26.5 eV. Otherwise, with all valance electrons of Pb, Ti and O atoms (i.e. $N = 50$), the free electron plasmon would be 33.0 eV. We will also see from sum rule data that $N = 34$ is a reasonable value for the valance electrons per (PT) molecule.

At low energy the transitions have been taken into account from:

O-2p → Ti-3d (t_{2g}) Pb-6s → Ti-3d(t_{2g})
O-2p → Ti-3d(e_g) Pb-6s → Ti-3d(e_g)
O-2p → Pb-6p Pb-6s → Pb-6p

The contribution from Ti-4s and Pb-4f are so small can be neglected and participation from Pb-5d and O-2s because have a narrow bands separated from the valance band by nearly 18 eV are rather weak. Therefore the totals of 6 are the major bands that contribute. A simplified energy level diagram to show these transitions at low energy is shown in Figure 7.

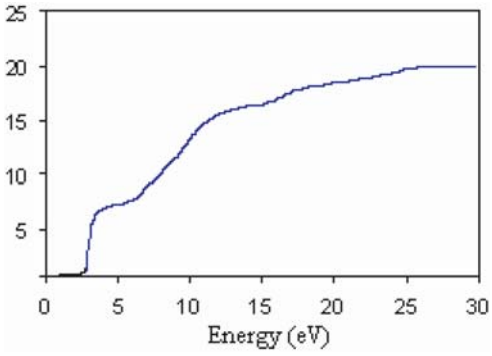

Fig. 8. Calculated oscillator strength sum rule for (PT) in cubic phase.

3.1.3 Oscillator strength sum rule

Another way to consider the number of electrons involved in the valance interband transition is to evaluate the sum rule. The effective number of valance electron per unit cell contributing to a transition up to frequency ω can be calculated using the sum rule [7]:

$$n_{eff}(\omega) = \int_0^{\omega} \sigma(\omega')\omega' \mathrm{d}\omega'. \quad (8)$$

The oscillator strength sum rule for (PT) is shown in Figure 8. The effective electron number up to 2 eV is zero (below band gap) then rises rapidly at low energy and saturates at about 20 eV, with a value of 18.1 for the effective electron number. However, in this transition, the contribution of O-2p bands to n_{eff} (E) is the largest, followed by Ti=O hybridized bands, and finally the Pb-4f, Ti-4s and O-2s bands contribution which is least.

The relatively small $n_{eff}(E)$ confirms, to some extent, the assumption that we may ignore the contribution of the Pb-5d and O-2s states. This is due to the stronger localization of deep laying these states, which inhibits transfer at low energies to high-energy interband transitions (Fig. 6).

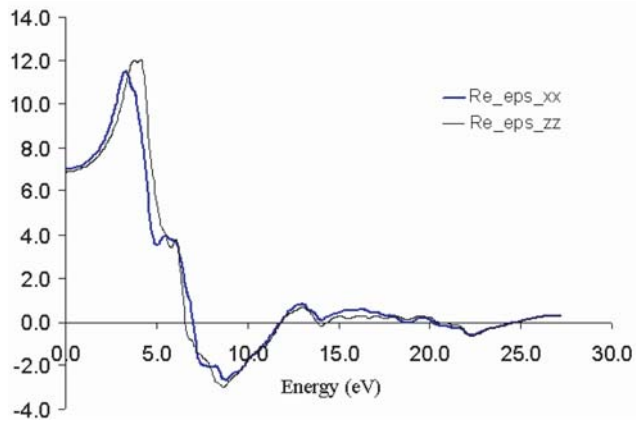

Fig. 9. Real part of dielectric function for (PT) in tetragonal phase along the a and c crystallographic axes.

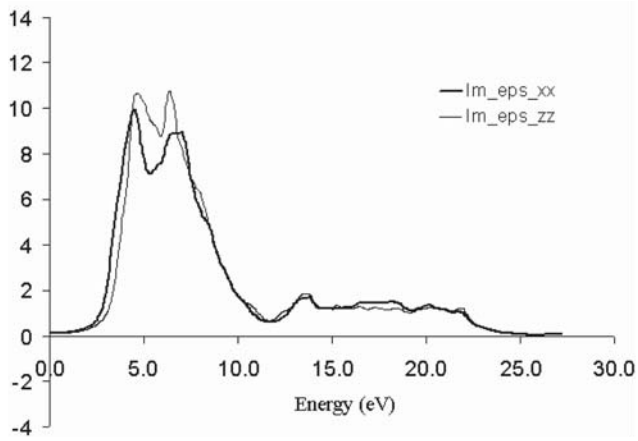

Fig. 10. Imaginary part of dielectric function for (PT) in tetragonal phase along the a and c crystallographic axes.

3.2 Ferroelectric phase

3.2.1 Dielectric function

Figures 9 and 10 show the real and imaginary parts of the dielectric functions for (PT) in tetragonal phase along the $a(-x)$ and $c(-z)$ crystallographic axes.

The general behavior of $\varepsilon_1(\omega)$ for the tetragonal phase curve is similar to that for the cubic phase. The static dielectric constant for the tetragonal phase has been decreased to 6.45. The main peak of $\varepsilon_2(\omega)$ for tetragonal phase curve has two peaks in the range of 4–8 eV.

The real and the imaginary parts of the optical conductivity are shown in Figures 11 and 12 for (PT) in the tetragonal phase along the $a(-x)$ and $c(-z)$ crystallographic axes.

In Figure 13 the optical constant $n_a(\omega)$ and $k(\omega)$ is shown for (PT) in tetragonal phase along $a(-\mathrm{x})$ crystallographic axis .

Referring to Figure 1, it can be seen that the calculated refractive index (n_a) for the tetragonal phase is 2.59 and is smaller than the value in the cubic phase.

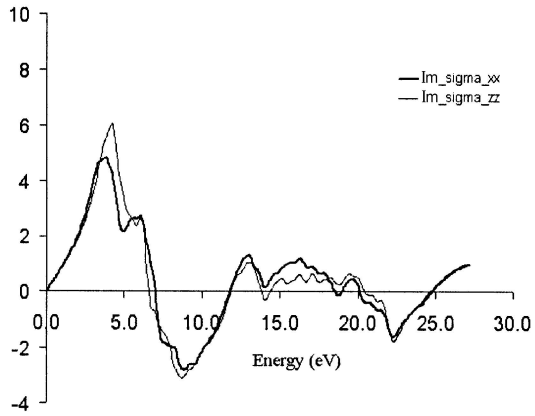

Fig. 11. Imaginary part of optical conductivity for (PT) in the tetragonal phase along the a and c crystallographic axes.

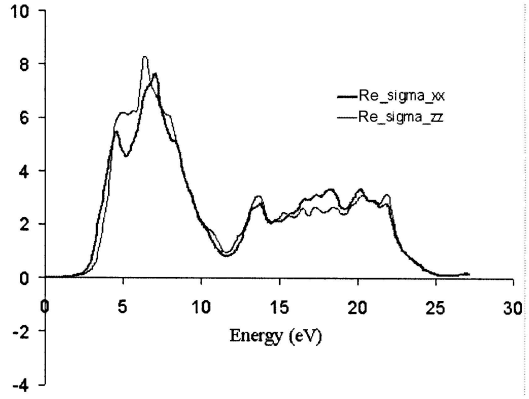

Fig. 12. Real part of optical conductivity for (PT) in the tetragonal phase along the a and c crystallographic axes.

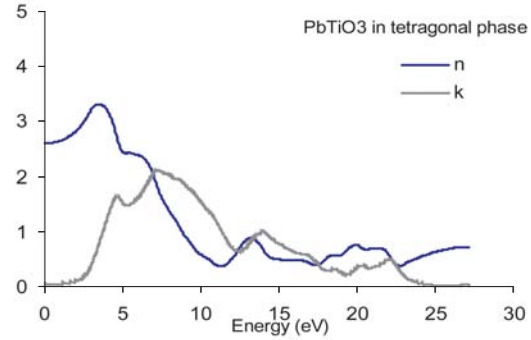

Fig. 13. The optical constant $n_a(\omega)$ and $k(\omega)$ for (PT) in tetragonal phase along the $a(-\mathrm{x})$ crystallographic axis.

The refractive index value for (PT) in tetragonal phase calculated in this work, and the values obtained by other methods are summarized in Table 3.

3.2.2 Electron energy loss spectroscopy

In Figure 14 the energy loss function is plotted for tetragonal phase. The energy of the main maximum of $\mathrm{Im}[-\varepsilon^{-1}(\mathrm{E})]$, or the energy of volume plasmon $\hbar\omega_p$, for

Table 3. (PT) static refractive index in cubic phase calculated by various methods.

Methods	Static refractive index (n_a)
Experimental	
Thin film by K MOCVD method at 632.8 nm [13]	∼2.64
Thin film by metalorganic chemical vapor at 800 nm [14]	∼2.35
Single crystal at 632.8 nm [15]	∼2.7
Theory	
point-dipole approach at 488 nm [16]	∼2.77
FP-LAPW (GGA96) (this work) at 465 nm	∼2.64
FP-LAPW (GGA96) (this work) at 643 nm	∼2.62
FP-LAPW (GGA96) (this work) at 830 nm	∼2.61

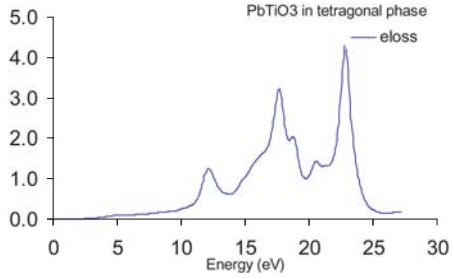

Fig. 14. Calculated EELS for (PT) in tetragonal phase.

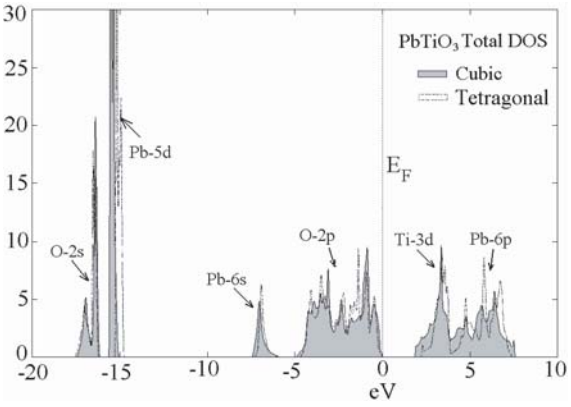

Fig. 15. Calculated total DOS for (PT) in tetragonal phase.

the tetragonal phase is smaller than cubic phase and equal 22.7 eV. The calculated band Structure shows the electronic band structure for the tetragonal phase yield an indirect band gap of 2.0 eV at X-Γ direction as reported somewhere else [7]. In comparison to cubic phase the top valance band due to hybridization along the polar c-direction is pushed down. The others two peaks are at 17.6 eV and 12.1 eV

As we can see from the total DOS of tetragonal phase, Figure 15, the Pb-5d and O-2s deep lying states are localized and the probability to transfer at low energy to high-energy interband transitions is less likely.

3.2.3 Oscillator strength sum rule

Figure 16 shows the n_{eff} (E) for (PT) in tetragonal phase. The curve is similar to that of cubic phase, the number

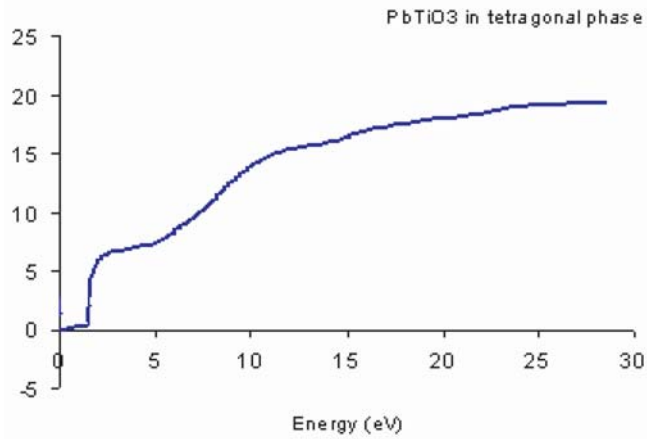

Fig. 16. Calculated oscillator strength sum rule (PT) in tetragonal phase.

of effective electron, $n_{eff}(E)$, rises rapidly at low energy to a value near 4 eV, and then there is another rise, and finally, saturation at a value near 20 eV with a value of 18 for the effective electron number. However, in this transition, the contribution O-2p to Ti-3d and Pb-6p orbitals, respectively to $n_{eff}(E)$ is most dominated.

4 Conclusions

We have calculated the optical properties of (PT) in cubic and tetragonal phases using the full potential–linearized augmented plane wave (FP-LAPW) method with the generalized gradient approximation (GGA). The calculations show a static refractive index of 2.81 and an EEL spectrum of 22.9 eV for the cubic phase. The effective electron number at low energy saturates near 20 eV with the value of 18.1 for the effective electron number. In the tetragonal phase the static refractive index has reduced to 2.59. The effective electron number for ferroelectric phase is the same for paraelectric phase. Ignoring the contribution of $5d^{10}$ and $2s^2$ electron of Pb and O atom respectively, then we have $N = 34$ and the free electron plasmon energy will be 23.4 eV. It seems that $N = 34$ is a reasonable value for the valance electrons per (PT) molecule.

The authors are grateful to Professor P. Blaha (at Vienna University of Technology Austria) for his technical assistance in the use of Wien2k package.

References

1. P. Blaha, D. Singh, P.I. Sorantin, K. Schwarz, Phys. Rev. B **46**, 1321 (1992)
2. J.F. Scott, C.A. Paz de Araujo, Science **246**, 144 (1986)
3. R.J. Nelmes, W.F. Kuhs, Solid State Commun. **54**, 721 (1985)
4. J.P. Perdew, J.A. Chevary, S.H. Vosko, K.A. Jackson, M.R. Pederson, D.J. Singh, C. Fiolhais, Phys. Rev. B **46**, 6671 (1992)
5. M. Peterson, F. Wanger, L. Hufnagel, M. Scheffler, P. Blaha, K. Schwarz, Comput. Phys. Commun. **126**, 294 (2000)
6. P. Blaha, K. Schwarz, WIEN2k, Vienna University of Technology Austria (2002)
7. F. Wooten, *Optical properties of solids* (Academic Press, New York, 1972)
8. S.M. Hosseini, T. Movlarooy, A. Kompany submitted for press
9. U.V. Waghmare, K.M. Rabe, Phys. Rev. **55**, 6161 (1997)
10. W. Kleemann, F.J. Schäfer, D. Rytz, Phys. Rev. B **34**, 7873 (1986)
11. E.R. Leite, L.P.S. Santos, N.L.V. Carreo, E. Longo, C.A. Paskocimas, J.A. Varela, F. Lanciott, C.E.M. Campos, P.S. Pizam, Appl. Phys. Lett. **78,** 2148 (2001)
12. S. Loughin, R.H. French, L.K. De Noyer, W.-Y Ching, Y.-N Xu J. Phys. D: Appl. Phys. **29**, 1740 (1996)
13. X.T. Chen, H. Yamane, K. Kaya, J. Phys. III France **2**, 1439 (1992)
14. M.P. Moretm M.A.C. Devillers, K. Worhoff, P.K. Larsen J. Appl. Phys. **92**, 468 (2002)
15. S. Singh, J.P. Remeika, J.R. Potopowicz, Appl. Phys. Lett. **20**, 135 (1972)
16. K. Bammou, D. Khatib, F. Bensamka, MJCM, **2** (1) art15 (1999)